

# Contents

- 7 Preliminary Study of the use of a Prognostic Model to Assess Pollutant Transport During WHITEX** **7-1**
- 7.1 The Model 7-1
- 7.2 The Meteorological Model Simulation of the WHITEX Area 7-1
- 7.3 The Dispersion Model Simulation 7-9
- 7.4 Conclusions 7-9

# List of Figures

7.1	Terrain used in the WHITEX area model simulation. . . . .	7-3
7.2	Thermodynamic soundings at Page. . . . .	7-4
7.2	Continued. . . . .	7-5
7.3	Simulated horizontal wind fields and vertical cross sections of vertical motion and potential temperature. . . . .	7-6
7.3	Continued . . . . .	7-7
7.4	Vertical cross section of potential temperature and simulated horizontal wind fields.	7-8
7.5	Simulated horizontal wind fields. . . . .	7-10
7.6	Location of particles from a continuous release as influenced by the simulated meteorological wind and turbulence fields. . . . .	7-11
7.7	A vertical cross section of particles from a continuous release as influenced by the simulated meteorological wind and turbulence fields. . . . .	7-12
7.8	Plume positions of regional sources as represented by a volume release. . . . .	7-13

## Chapter 7

# Preliminary Study of the use of a Prognostic Model to Assess Pollutant Transport During WHITEX

### 7.1 The Model

A prognostic meteorological model is based on fundamental conservation principles of velocity, heat, mass, and moisture. Mathematical relations are constructed, and then approximated on a discrete model grid in order to represent and diagnose atmospheric conditions at a given time, and to predict the subsequent behavior of the atmosphere. Since the model equations are based on fundamental conservation principles, as described in Pielke,<sup>6</sup> the velocity, heat, mass, and moisture fields are internally consistent with one another.

The use of a prognostic meteorological model to assess pollutant transport has the following advantages as contrasted with current Environmental Protection Agency regulatory models.

1. Physically consistent meteorological fields can develop, through nonlinear interactions, on a spatial scale smaller than can be resolved from the standard synoptic observation network, or even from the special meteorological monitoring network in WHITEX.
2. Physically consistent meteorological fields can also develop as a result of inhomogeneities in the surface forcing (e.g. sloping terrain, variable land use). The atmospheric response to these inhomogeneities could not be simulated without the characterization of the surface forcing and the prognostic meteorological model.

In this study, we used the meteorological model originally developed by Pielke,<sup>5</sup> and modified as reported in Mahrer and Pielke,<sup>2</sup> McNider and Pielke<sup>4</sup> and elsewhere. The dispersion model used, and which is linked to the output of the meteorological model, was developed originally by McNider.<sup>3</sup> The use of this model to simulate transport and dispersion has been reported in, for example, Pielke et al.,<sup>7</sup> Segal et al.,<sup>8</sup> and Yu and Pielke.<sup>9</sup>

### 7.2 The Meteorological Model Simulation of the WHITEX Area

The model is currently being applied to the WHITEX area in order to address the question of the influence of the local terrain, and its diurnal heating on the prevailing synoptic flow. The

climatological frequency of different synoptic flows during the winter season has been reported in Chapter 2.

The model domain is illustrated in Figure 7.1 where the terrain is contoured in intervals of decameters. The dashed line in the Figure is the Colorado River.

As our preliminary test of the model, we are simulating the February 11-12, 1987 period of WHITEX. The thermodynamic and wind sounding from Page at 0600 LST, 1100 LST, and 1700 LST on February 11 and at 0600 LST and 1100 LST on February 12 (Figures 7.2a-e) document a nearly adiabatic layer during the day up to about 800 mb capped by a very stable layer for up to several hundred meters, with a less stable layer further aloft.

The atmosphere throughout the depth of the sounding was quite moist for this time period. The observed winds below the inversion were generally from the northeast with southwest winds above the inversion. The synoptic classification based on National Weather Service surface pressure analyses for the February 11-12, 1987 time period indicated that the lower level winds at Page resulted from the positioning of the Great Basin High to the north of the WHITEX area.

The model input parameters for this preliminary run included the following characteristics:

- Horizontal grid spacing equal to 5.5 km with 69 by 69 horizontal grid points.
- 18 grid points in the vertical with the highest resolution in the lower troposphere and with a model top at 9 km, and the tropopause at about 7.5 km. An absorbing layer was prescribed near the model top to eliminate downward reflection of upward propagating gravity waves.
- A time step of 60 seconds.
- An initial temperature and moisture lapse rate of  $7.3^{\circ}\text{C km}^{-1}$ ,  $3.7^{\circ}\text{C km}^{-1}$ , and  $17.2^{\circ}\text{C km}^{-1}$ , and  $3.0 \text{ g kg}^{-1}$ ,  $1 \text{ to } 2 \text{ g kg}^{-1}$ , and  $0.5 \text{ g kg}^{-1}$  for the layers surface to 1.5 km, 1.5 km to 7.0 km, and 7.0 to 9.0 km, respectively.
- An initial wind flow of  $2 \text{ m s}^{-1}$  from the northeast up to 700 m above the lowest model elevation ( $\sim 150 \text{ m}$  below the Page elevation) with the speed linearly decreasing to zero at 1.1 km above this lowest elevation. See Appendix 8A for the surface pressure fields for this time which helps explain the observed low-level northeast flow.
- A surface albedo for the region of 0.5 as determined from satellite imaging due to the presence of mid-level cloud cover and snow cover at the surface.

Several illustrative meteorological simulated fields are presented in Figures 7.3a-d. Figures 7.3a and b show that even with prevailing light northeast geostrophic winds, the diurnal heating of the terrain induces major directional and speed perturbations to the flow even up to 500 m. Note, for instance, the upslope flows associated with the Kaibab Plateau, including the acceleration of the northeast flow from Page toward Hopi Point. A vertical cross section of potential temperature through this region at 1500 LST at  $36.7^{\circ}\text{N}$  indicates that the heating of the surface and resultant convective mixing is unable to eliminate the strong capping inversion at 800 mb (the time-lapse video images for February 11 and 12 clearly show that the inversion was well defined throughout this period). Only in association with highest terrain features (e.g. see Figures 7.3d and e) was there any significant coupling between the flow aloft and the air below the inversion.

By 2100 LST (e.g. see Figure 7.4a), long wave radiational cooling near the surface becomes dominant and the low-level stable layer is reestablished. The simulated winds at 8 m and 500 m at this time are shown in Figures 7.4b and c. Even though the winds have become weaker at 8m and suggest the development of drainage flow, substantial flow from the northeast from Page at 500 m

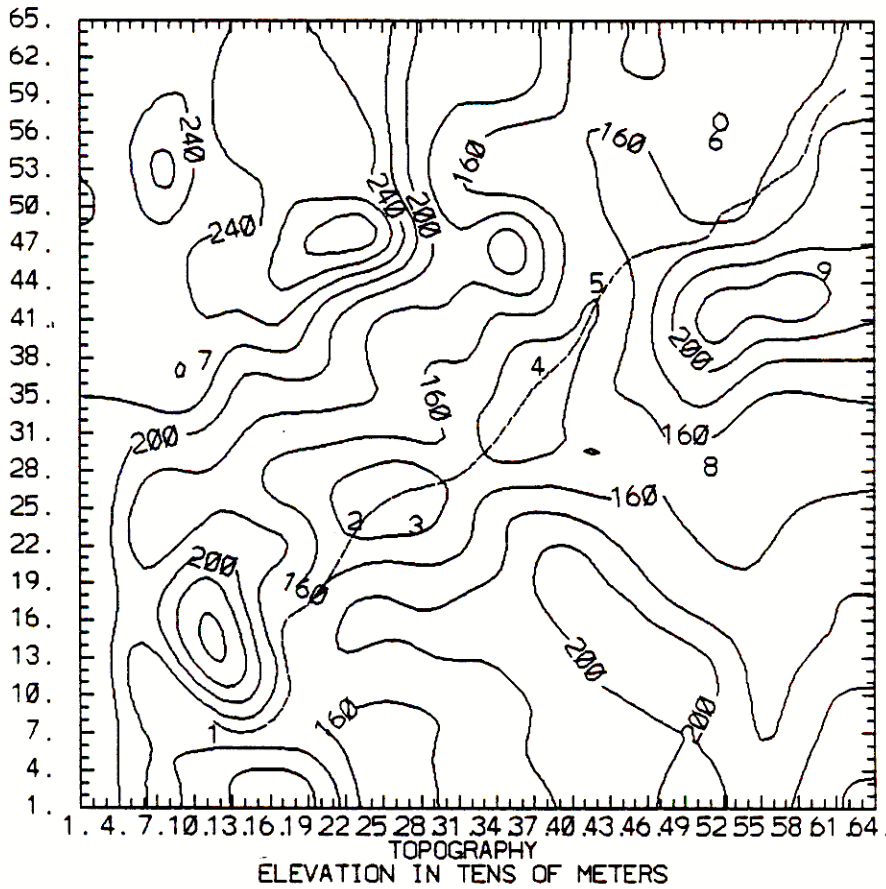


Figure 7.1: Terrain used in the WHITEX area model simulation at 1) Hopi Point; 2) Page; 3) Navajo Generating Station (NGS); 4) Bullfrog; 5) Hite; 6) Canyonlands; 7) Bryce; 8) Mexican Hat; and 9) Monticello.

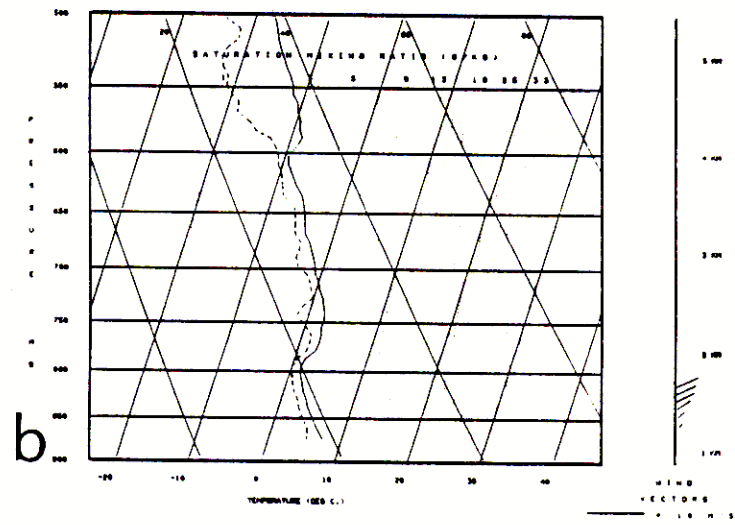
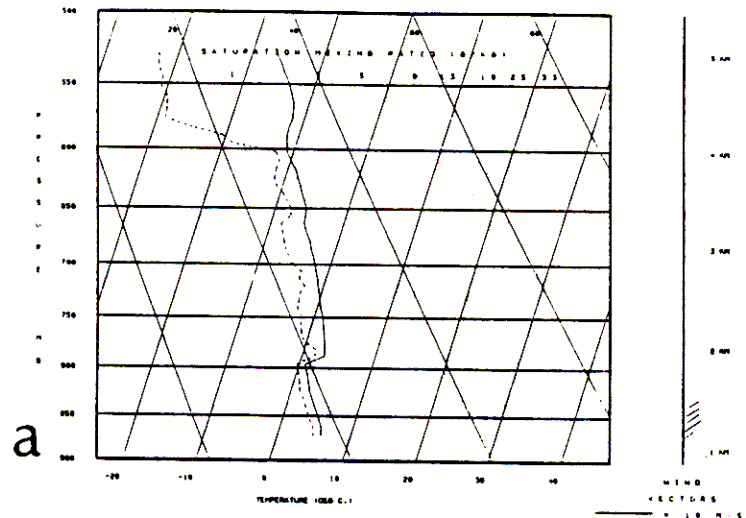


Figure 7.2: Thermodynamic sounding at Page at (a) 0600 LST on February 11, 1987; and (b) 1100 LST on February 11, 1987.

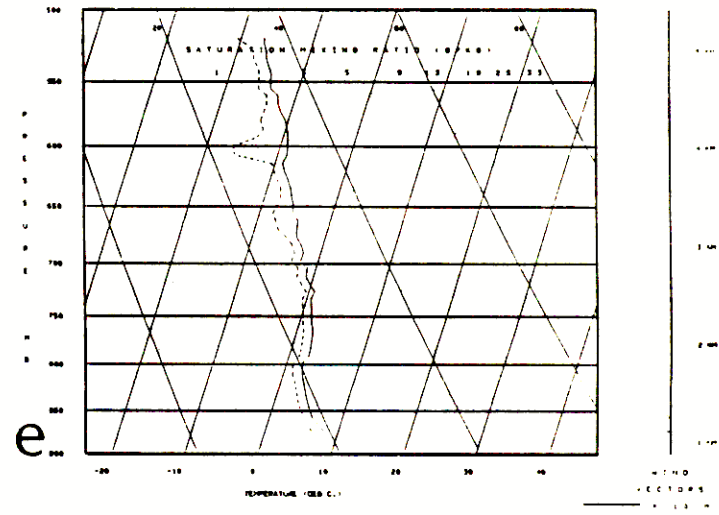
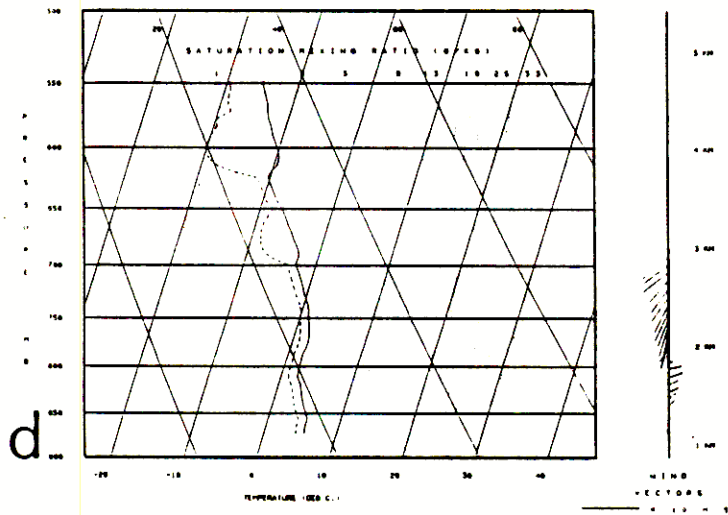
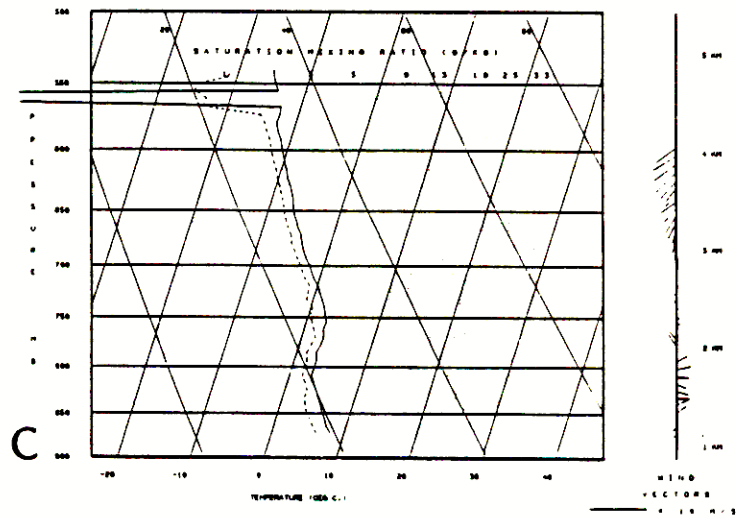


Figure 7.2: Continued: (c) 1700 LST on February 11, 1987; (d) 0600 LST on February 12, 1987; and (e) 1100 LST on February 12, 1987.

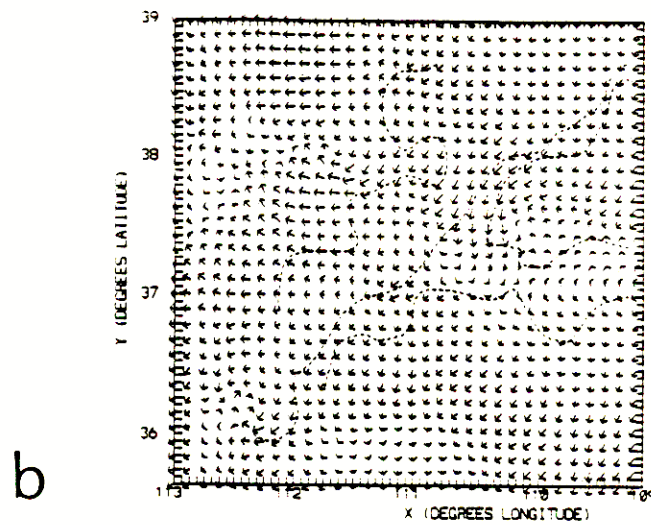
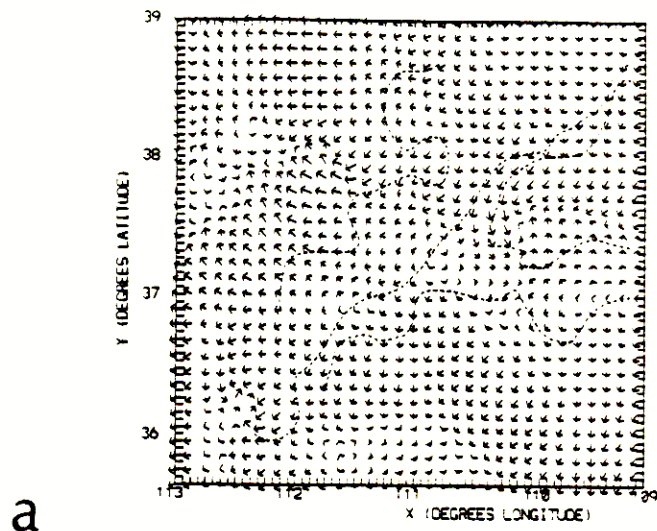


Figure 7.3: Simulated horizontal wind field at 1500 LST at (a) 8 m above the surface; and (b) 500 m above the surface. (The distance between each tick mark represents an arrow speed of  $4 \text{ m s}^{-1}$ .)

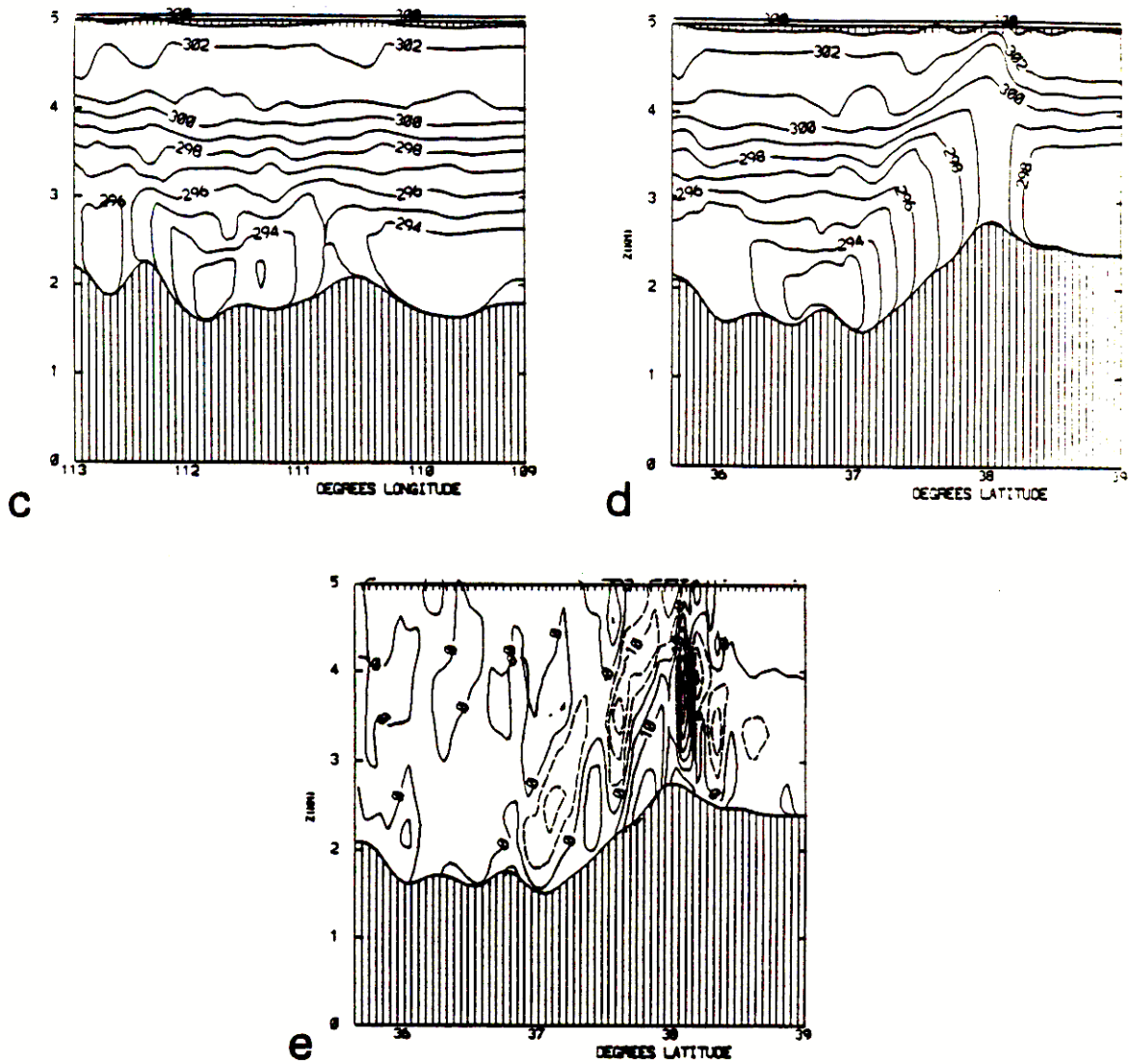


Figure 7.3: Continued: Vertical cross section of (c) potential temperature in Kelvin at 1500 LST at latitude 36.7°N; (d) potential temperature in Kelvin at longitude 111.7°W; and (e) vertical velocity ( $\text{cm s}^{-1}$ ) at longitude 111.7°W with dashed lines indicating downward motion and solid lines indicating upward motion.

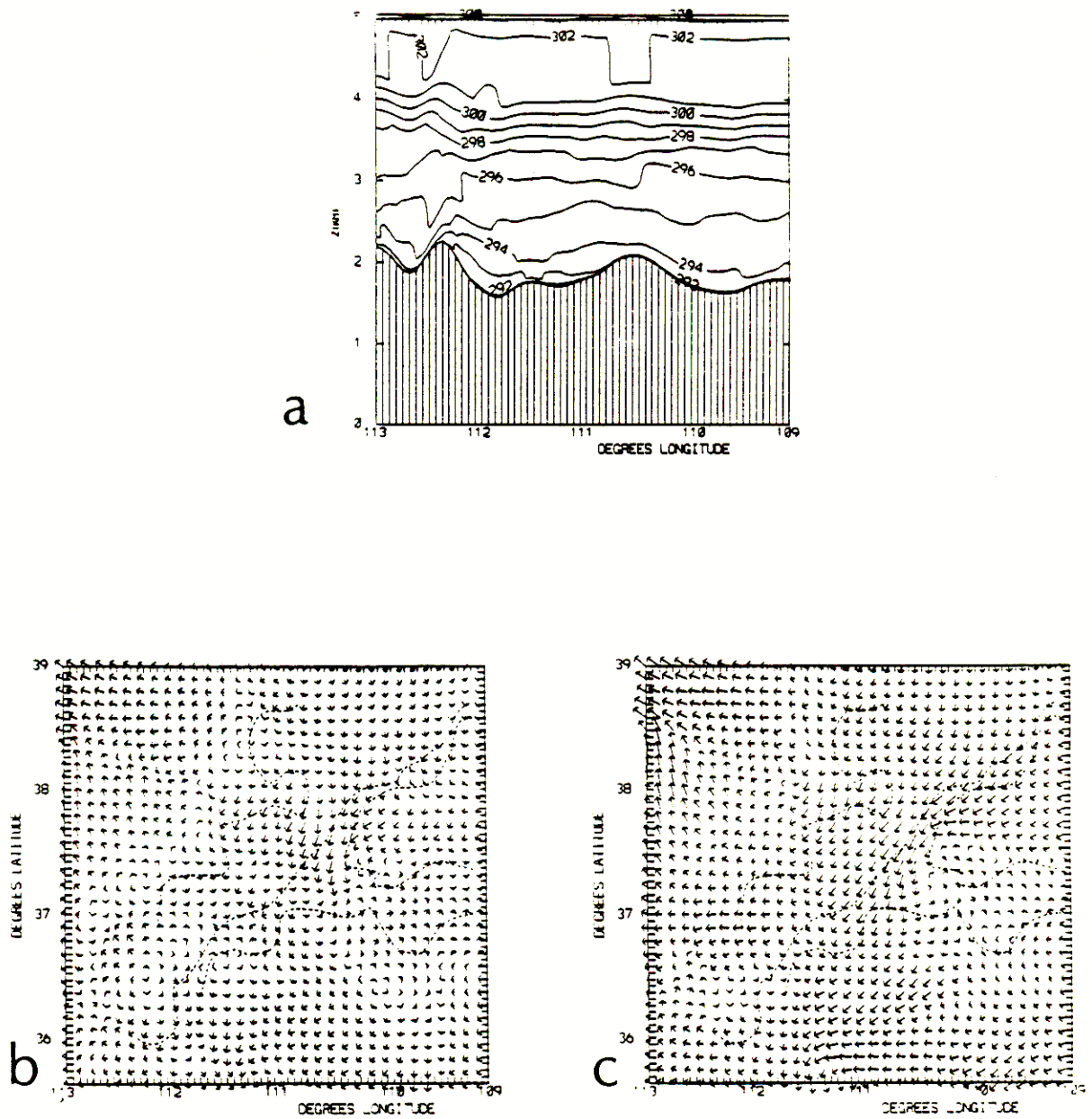


Figure 7.4: (a) Vertical cross section of potential temperature in Kelvin at 2100 LST at latitude 36.7°N; (b) simulated horizontal wind field at 2100 LST at 8 m above the surface; and (c) simulated horizontal wind field at 2100 LST at 500 m above the surface. (The distance between each tick mark represents an arrow speed of  $4 \text{ m s}^{-1}$ .)

towards the Hopi Point area persists. Figures 7.5a-d show that this southwest movement of air at 500 m persisted throughout the night into the next morning.

### 7.3 The Dispersion Model Simulation

Using the three-dimensional wind and turbulence field simulated by the meteorological model, a lagrangian particle model is used to estimate the movement and spread of material which is released from the effective stack height ( $\sim 600$  m) of Navajo Generation Station (NGS), and to evaluate transport into the region from more distant sources. Particles were released continuously at a rate of 18 particles per hour for the 24-hour simulation. Concentration estimations can be obtained from a continuous release and be compared with observations. This was not done here due to the large number of particles needed to adequately characterize the concentrations. This section is meant only to visualize the overall plume movement.

Figures 7.6a-i show the movement of the simulated pollution at several hour intervals which was initially released at 1000 LST from NGS. Asterisks indicate reference points with the locations being the same as those given in Figure 7.1. As expected from the output of the meteorological fields, the general movement of the material is towards the southwest. At night, the lateral spread of the plume is much less as a result of the thermodynamic stabilization due to long-wave radiational cooling. A vertical cross section looking north with the terrain configuration at latitude  $36.7^\circ\text{N}$  at the same times as in Figures 7.6a-h is given in Figures 7.7a-h. The vertical spread of the plume up to the inversion height during the day, and its confinement to a narrow layer at nights is quite evident in the Figures. The movement of the simulated pollution to the west is also clear.

Finally, Figures 7.8a-c show the movement of particles released instantaneously through a depth of 800 m above the surface at four locations within the domain. These releases are designed to represent sources of pollution to the south, east-northeast, and northeast of Hopi Point, as well as from NGS. The movement of effluent from the Page area toward Hopi Point is again clearly evident, as was already seen in Figures 7.6a-i. The southern pollutant mass, even though artificially placed close to Hopi Point, quickly advects out of the region. The source to the east-northeast remains in that area because of the local wind field in that area which is strongly perturbed by the thermally-forced terrain flow in that area. Only the northern source moves towards the southwest and would be expected to impact Page if this synoptic flow pattern persisted long enough. Therefore, only sources to the north of Hopi Point would be expected to impact the Grand Canyon for an instantaneous release at 1000 LST.

### 7.4 Conclusions

This preliminary model simulation has assisted in explaining how material can be transported towards Hopi Point from NGS. The light synoptic northeast flow coupled with thermally-induced winds associated with the Kaibab Plateau act to transport material towards the southwest. At night, even though the lowest levels become influenced by drainage winds and a stable thermodynamic stratification, at 500 m the northeast flow from NGS to Hopi point persists.

Thus, based on this model experiment, *NGS was a major contributor to the sulfur observed at Hopi Point on February 11 and 12, 1989.* An NGS plume could be expected to reach Hopi Point in approximately 12 hours for these two days.

In addition, for these two days, only transport of sulfur from the north of Page could contribute to the sulfur load at Hopi Point although transport times of 2 days or longer seem to be required under this synoptic regime.

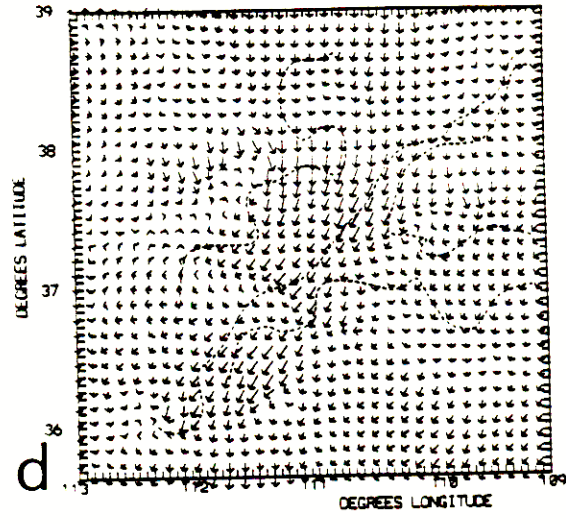
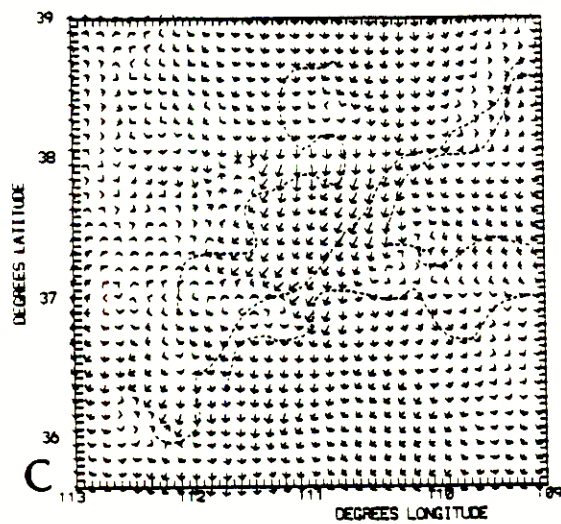
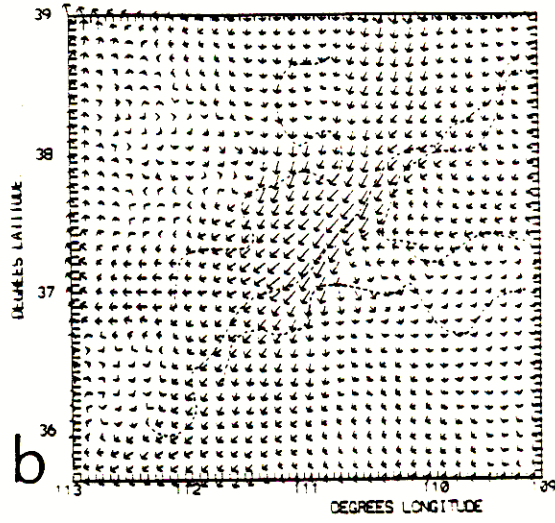
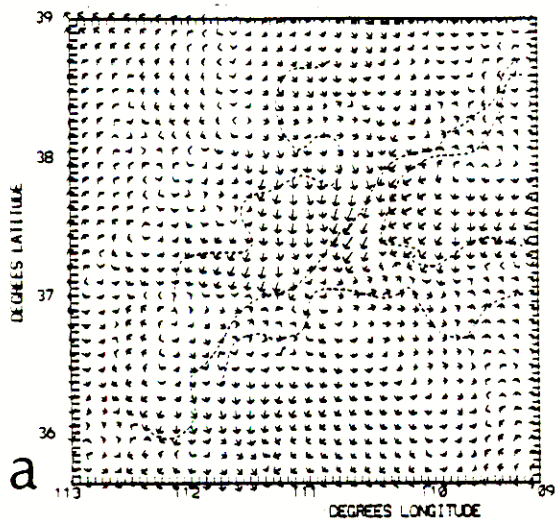


Figure 7.5: Simulated horizontal wind field at (a) 8 m above the surface at 0300 LST the following day; (b) 500 m above the surface at 0300 LST the following day; (c) 8 m above the surface at 0900 LST the following day; and (d) 500 m above the surface at 0900 LST the following day. (The distance between each tick mark represents an arrow speed of  $4 \text{ m s}^{-1}$ .)

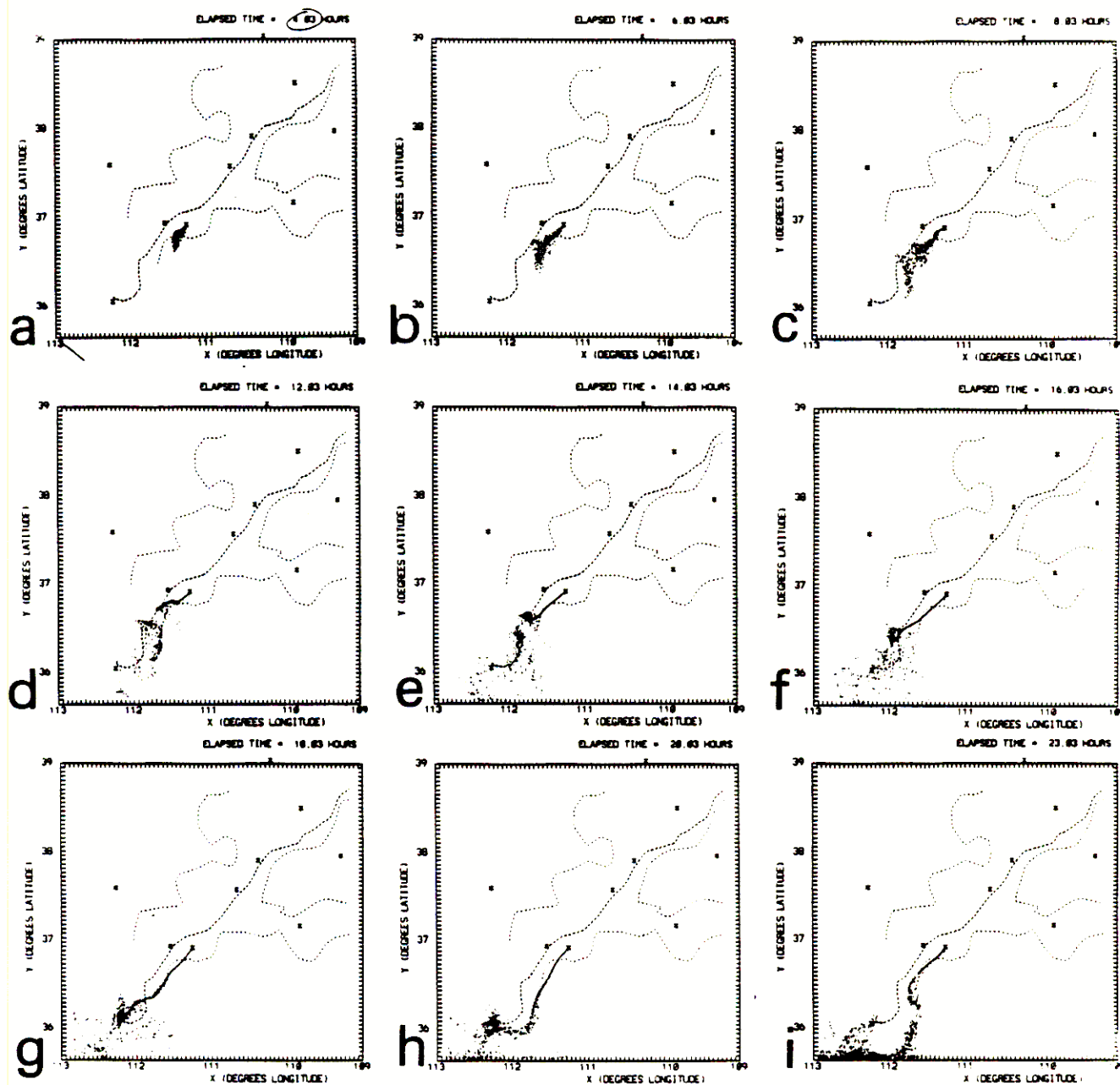


Figure 7.6: Location of particles from a continuous release which began at 1000 LST as influenced by the simulated meteorological wind and turbulence fields at: (a) 1400 LST; (b) 1600 LST; (c) 1800 LST; (d) 2200 LST; (e) 0000 LST; (f) 0200 LST; (g) 0400 LST; (h) 0600 LST; and (i) 0900 LST.

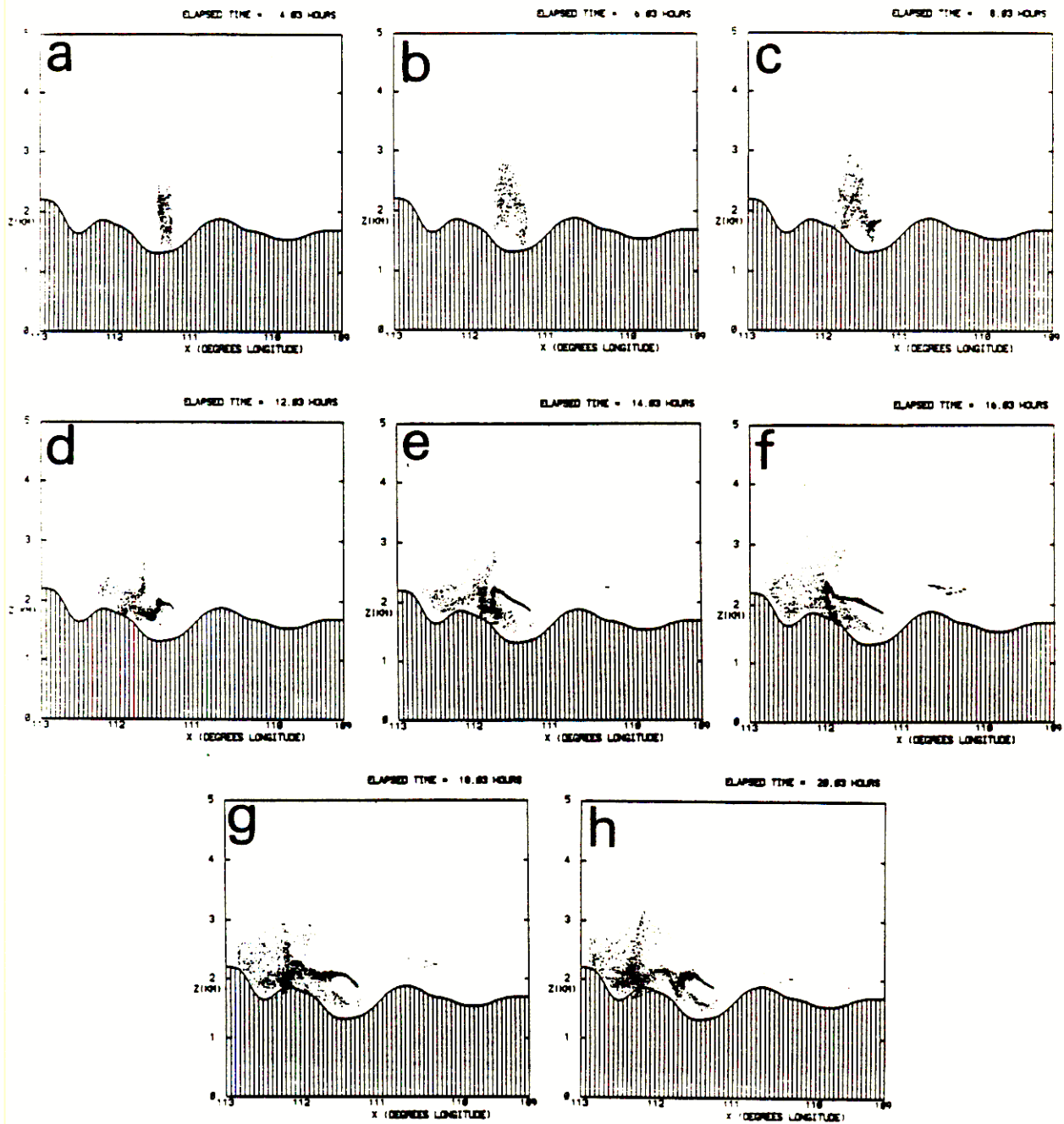


Figure 7.7: A vertical cross section of particles from a continuous release which began at 1000 LST as influenced by the simulated meteorological wind and turbulence fields at (a) 1400 LST; (b) 1600 LST; (c) 1800 LST; (d) 2200 LST; (e) 0000 LST; (f) 0200 LST; (g) 0400 LST; (h) 0600 LST; and (i) 0900 LST. (Note that particles can appear below the terrain shown here since the view is of all particles at a given longitude in the model domain and elevations lower than shown do occur.)

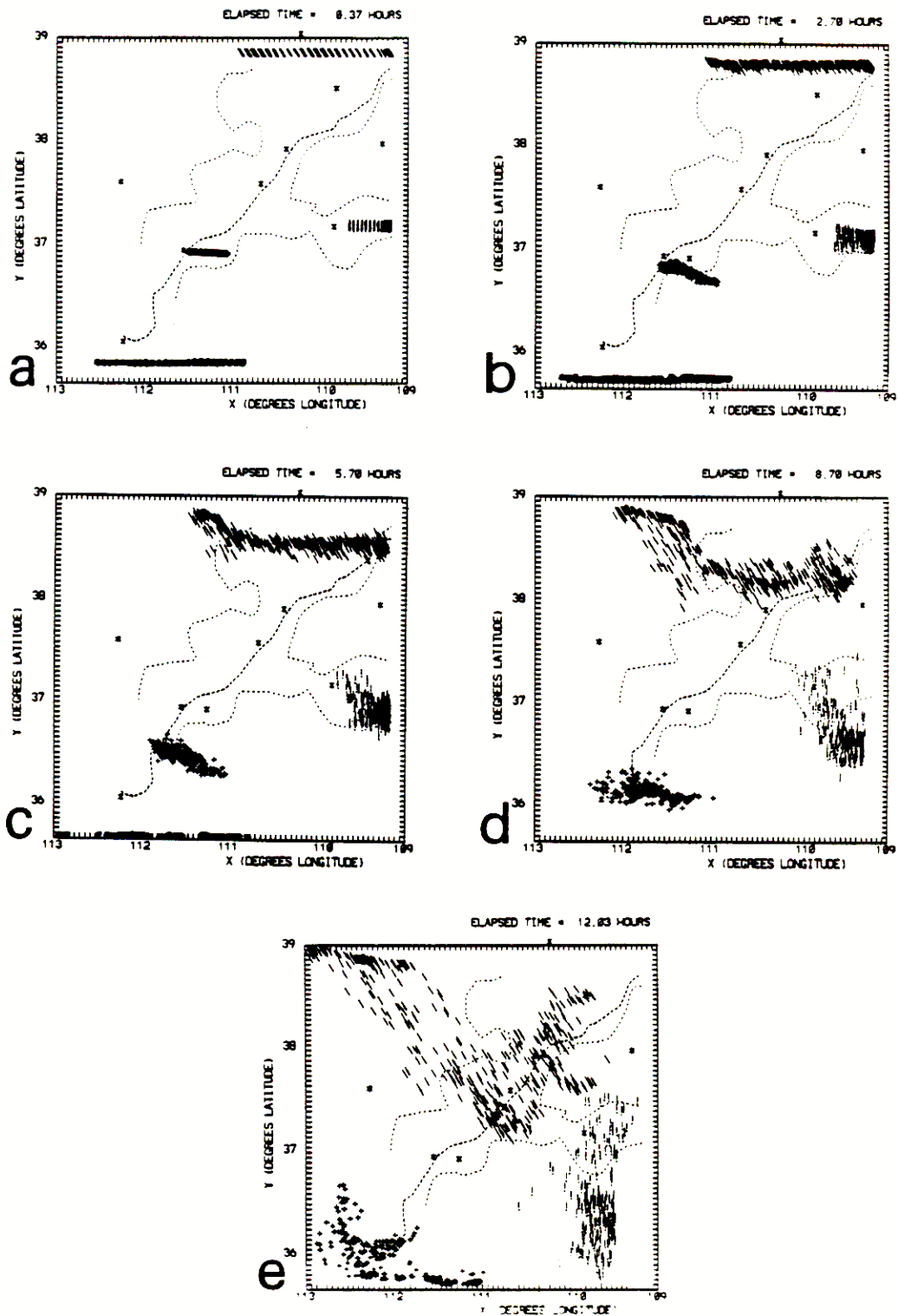


Figure 7.8: Plume position of regional sources as represented by a volume release of pollution which began at 0940 LST at a depth of 800 m at (a) 1000 LST; (b) 1200 LST; (c) 1500 LST; (d) 1800 LST; and (e) 2130 LST.

Current plans are to extend this work to include the observed southwesterlies aloft, and to run the new version of our modeling system (RAMS-Regional Atmospheric Modeling System<sup>1</sup>) which will permit us to vary the synoptic conditions as well as to simultaneously focus down to the Page-Hopi Point area using a telescoping two-way interactive grid nest. This latter enhancement will permit us to model longer period events and to include a more detailed representation of the terrain.

The southwesterlies aloft are not expected to significantly influence our current simulation of February 11 and 12, 1987 since, as evident in the time-lapse movies and in Figure 7.2, the lower layer was obviously decoupled from the flow at higher levels. The persistence of the inversion at around 800 m clearly documents that little mixing could have occurred across this layer even during the daytime - otherwise the inversion would have been removed and replaced by an adiabatic layer.

## References

- <sup>1</sup>Cotton, W.R., R.A. Pielke, C.J. Tremback, R.L. Walko, J. Cram, J. Verlinde, G.J. Tripoli, P.J. Flatau, M. Nicholls, M.J. Weissbluth, M. Moran, R. Avissar, W. Miller, and R. McNider, 1989: CSU RAMS – A multipurpose weather modelling system. *Environ. Software*, (in preparation).
- <sup>2</sup>Mahrer, Y. and R.A. Pielke, 1977: A numerical study of the air flow over irregular terrain. *Contrib. Atmos. Phys.*, **50**, 98-113.
- <sup>3</sup>McNider, R.T., 1981: Investigation of the impact of topographic circulations on the transport and dispersion of air pollutants. Ph.D. Dissertation, Department of Environmental Sciences, University of Virginia, 210 pg.
- <sup>4</sup>McNider, R.T. and R.A. Pielke, 1981: Diurnal boundary layer development over sloping terrain. *J. Atmos. Sci.*, **38**, 2198-2212.
- <sup>5</sup>Pielke, R.A. 1974: A three-dimensional numerical model of the sea breeze over south Florida. *Mon. Wea. Rev.*, **102**, 115-134.
- <sup>6</sup>Pielke, R.A., 1984: *Mesoscale meteorological modeling*. Academic Press, New York, N.Y., 612 pp.
- <sup>7</sup>Pielke, R.A., R.T. McNider, M. Segal and Y. Mahrer, 1983: The use of a numerical mesoscale model for evaluations of pollutant transport and diffusion in coastal regions and over irregular terrain. *Bull. Amer. Meteor. Soc.*, **64**, 243-249.
- <sup>8</sup>Segal, M., R.A. Pielke, R.W. Arritt, M.D. Moran, C-H. Yu and D. Henderson, 1988: Application of a mesoscale atmospheric modeling system to the estimation of  $SO_2$  concentrations from major elevated sources in southern Florida. *Atmos. Environ.*, **22**, 1319-1334.
- <sup>9</sup>Yu, C-H. and R.A. Pielke, 1986: Mesoscale air quality under stagnant synoptic cold season conditions in the Lake Powell area. *Atmos. Environ.*, **20**, 1751-1762.